Supplement of Atmos. Chem. Phys., 18, 6733–6748, 2018
https://doi.org/10.5194/acp-18-6733-2018-supplement

Atmospheric Chemistry and Physics
Open Access
EGU

Supplement of

Synoptic meteorological modes of variability for fine particulate matter ($PM_{2.5}$) air quality in major metropolitan regions of China

Danny M. Leung et al.

Correspondence to: Amos P. K. Tai (amostai@cuhk.edu.hk)

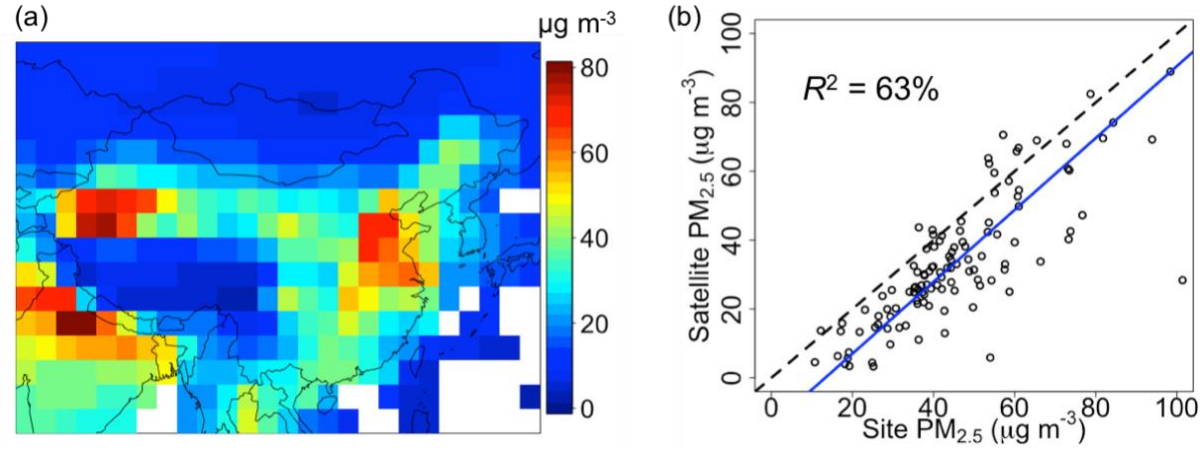

Fig. S1. Annual mean total $PM_{2.5}$ as derived from 2.5°×2.5° satellite observations in 1998–2015. AOD data from various satellite products are used to calculate annual mean $PM_{2.5}$ following van Donkelaar et al. (2016). (a) Averaged $PM_{2.5}$ in 1998–2015 over the whole China. Whitened gridboxes are due to the lack of satellite observations. (b) Annual mean satellite-derived $PM_{2.5}$ concentrations (μg m^{-3}) from van Donkelaar et al. (2016) versus gridded annual mean site $PM_{2.5}$ concentrations (μg m^{-3}) from the Chinese Ministry of Environmental Protection (MEP, http://pm25.in), for year 2015. The blue line indicates the fitted line using reduced major axis (RMA) regression with an R^2 value of 0.63, and the dashed line indicates the 1:1 line.

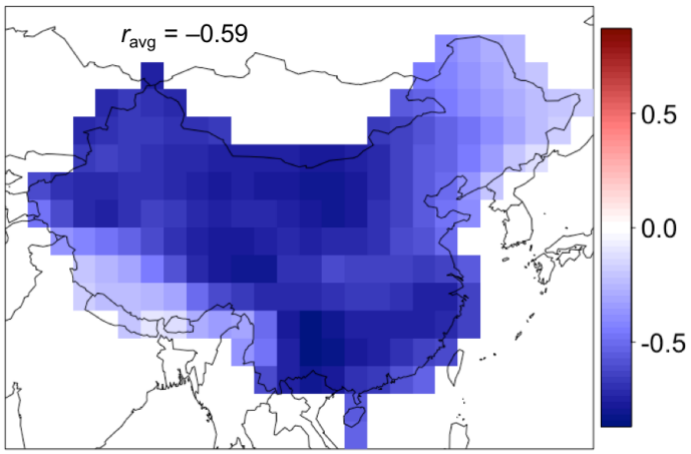

Fig. S2. Pearson's correlation map of 2.5°×2.5° deseasonalized surface air temperature (T, X_1 in Table 1) and sea level pressure (SLP, X_4 in Table 1) during the study period of June 2014 to May 2016. Text inset shows the correlation averaged over the entire China.

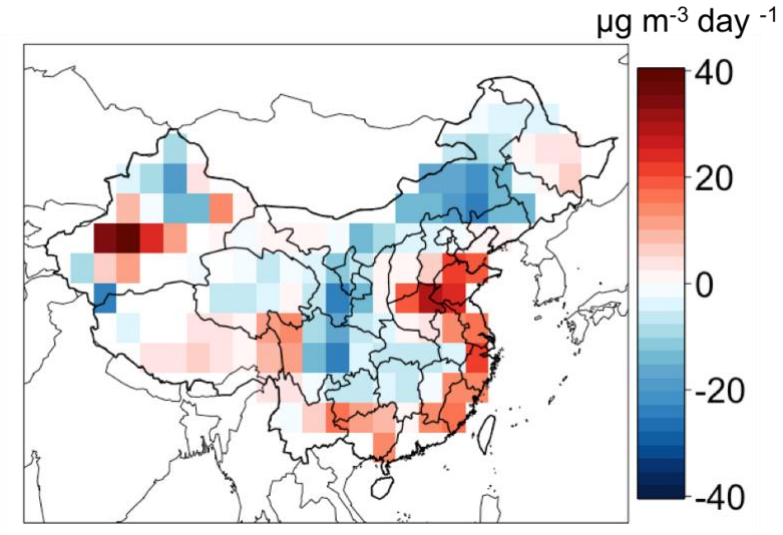

Fig. S3. Mass divergence map of $PM_{2.5}$ according to the continuity equation in Eulerian form $-\frac{\partial \rho}{\partial t} = \nabla \cdot (\rho \vec{V})$, which indicates the mass flux of $PM_{2.5}$ (divergence in red). ρ (μg m^{-3}) is the average mass concentration of $PM_{2.5}$, and $\vec{V} = (u, v)$ (m s^{-1}) is the correlation vector in Fig. 2(g). The map shows that the two strongest divergent patterns are over BTH and Xinjiang, where $PM_{2.5}$ is advected out of the grid cells. The two regions are surrounded by the light blue colors, indicating the peripheries are affected by pollution from the source regions.

Table S1. Models from the Coupled Model Intercomparison Project Phase 5 (CMIP5) used for this study.

Model name	Institute
CMCC-CESM	Centro Euro-Mediterraneo per i Cambiamenti Climatici
CMCC-CM	Centro Euro-Mediterraneo per i Cambiamenti Climatici
CMCC-CMS	Centro Euro-Mediterraneo per i Cambiamenti Climatici
CNRM-CM5	Centre National de Recherches Meteorologiques / Centre Europeen de Recherche et Formation Avancees en Calcul Scientifique
GFDL-CM3	Geophysical Fluid Dynamics Laboratory
GFDL-ESM2G	Geophysical Fluid Dynamics Laboratory
GFDL-ESM2M	Geophysical Fluid Dynamics Laboratory
HadGEM2-CC	Met Office Hadley Centre
HadGEM2-ES	Met Office Hadley Centre (Instituto Nacional de Pesquisas Espaciais)
INM-CM4	Institute for Numerical Mathematics
MIROC-ESM	National Institute for Environmental Studies
MIROC-ESM-CHEM	National Institute for Environmental Studies
MPI-ESM-LR	Max Planck Institute for Meteorology
MPI-ESM-MR	Max Planck Institute for Meteorology
MRI-ESM1	Meteorological Research Institute

1. Calculation of standard errors of meteorological composition

For each mode, we calculate the variances of meteorological composition by this formula:

$$\widehat{\boldsymbol{e}_{\boldsymbol{j}}} \sim N\left(\boldsymbol{e}_{\boldsymbol{j}}, \frac{\lambda_j}{n} \sum_{i=1, i \neq j}^{8} \frac{\lambda_i}{\left(\lambda_i - \lambda_j\right)^2} \boldsymbol{e}_{\boldsymbol{i}} \boldsymbol{e}_{\boldsymbol{i}}'\right)$$

where $\boldsymbol{e_j}$ is the meteorological composition (as an eigenvector) of the j^{th} PC, λ_j the variance (eigenvalue) of the j^{th} PC, n = 8 the total number of PC found. The diagonal elements of the covariance matrix are the variances of the modes. We find the standard errors of each element of the eigenvector, and then plot out the error bar of 95 % confidence level (two standard errors).

Table S2. Regression results of the principal component time series on $PM_{2.5}$ in the Beijing-Tianjin-Hebei (BTH). Statistically significant results are colored in red. NAs indicate PCs with variance smaller than 1.

Season	$PM_{2.5}$ variability explained (%)				Regression coefficient (μg m^{-3})			
	1st PC	2nd PC	3rd PC	4th PC	1st PC	2nd PC	3rd PC	4th PC
Winter	43.67	0.00	4.22	NA	–30.89	–1.03	–13.16	NA
Spring	16.52	18.00	0.13	2.72	–11.55	12.08	1.59	5.69
Summer	0.16	16.66	6.86	0.03	0.16	–8.71	6.68	–0.46
Fall	33.40	4.53	1.37	0.07	–22.95	–8.76	6.54	1.56
Annual	36.44	0.21	0.14	0.05	–22.42	–1.67	–1.67	1.03

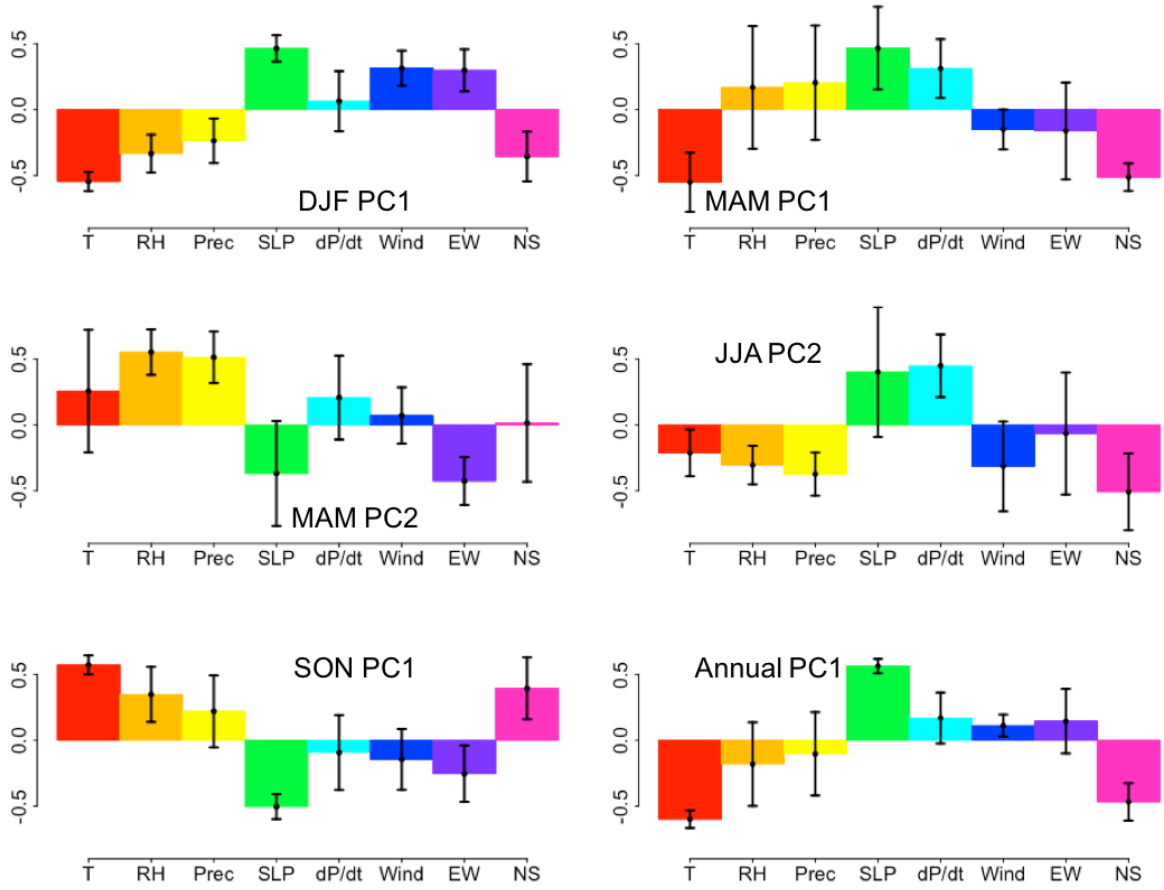

Fig. S4. Composition of the dominant principal components (PCs) for individual seasons and for the whole year in the Beijing-Tianjin-Hebei (BTH), corresponding to the red values in Table S2. We classify the second PC in spring as onshore flow associated with high ambient RH, the second PC in summer as southerly flow associated with high RH, and the rests as cold-frontal northerly wind from Siberian high. The panel showing the composition of annual PC1 is the same as Figure 3b. Error bars show two standard deviations of the distributions.

2. Seasonally dominant meteorological modes of $PM_{2.5}$ variability in the Beijing-Tianjin-Hebei (BTH)

In spring, there are two meteorological modes that together explain 34% of the springtime $PM_{2.5}$ variability. The first mode is also associated with the Siberian high (Fig. S5), with its meteorological composition close to that in winter (see Fig. S4). Figure S6 shows the second mode contributing to 18% of $PM_{2.5}$ variability in spring. The time series of this PC and deseasonalized $PM_{2.5}$ show a positive correlation (Fig. S5a). The EOF of this model consists of high RH, high precipitation, low SLP and easterly wind (Fig. S6b), with the positive phase representing moist conditions with high water content in ambient air together with some rainfall. The weather map (Fig. 6c) indicates that rainfall in BTH was about 3 mm d^{-1} on 16 Mar 2015, likely too weak to cause effective wet deposition of $PM_{2.5}$ even though the corresponding eigenvector coefficient for the normalized variable is large. Springtime easterly onshore wind brings moisture (> 70% RH) from the East China Sea, which may promote formation of semivolatile PM such as ammonium nitrate and organics (Dawson et al., 2007b). The weather map on 9 Mar 2015 (Fig. S6d) shows the negative phase of the mode when northwesterly wind is dominant and RH is less than 40%, helping ventilation and suppressing aqueous phase reactions of $PM_{2.5}$.

Figure S7 shows the only dominant mode in summer, explaining 17 % of the summertime $PM_{2.5}$ variability. The mode has strong correlation with $PM_{2.5}$ (Fig. S7a). The positive phase of this PC consists of high precipitation and RH and decreasing SLP and southerly wind (Fig. S7b), reflecting a southerly monsoonal flow, which brings moisture from the Pacific Ocean northward. Generally, a "Mei-yu" rain belt forms in central China when local southwesterly wind strengthens, with increased upward motion and water vapor convergence (Zhao et al., 2007). The weather map (Fig. S7c) shows a Mei-yu belt on 15 Jun 2015 in central China, which caused more than 20 mm d^{-1} of rainfall in Henan and Anhui provinces but little rainfall in BTH. This result implies that southerly wind could bring moisture and pollutants from high-emission regions to the north without effective wet deposition. The negative phase of this mode, however, brings increasing pressure tendency and northerly wind that can transport away $PM_{2.5}$ in a motion analogous to a cold front (Fig. S7d).

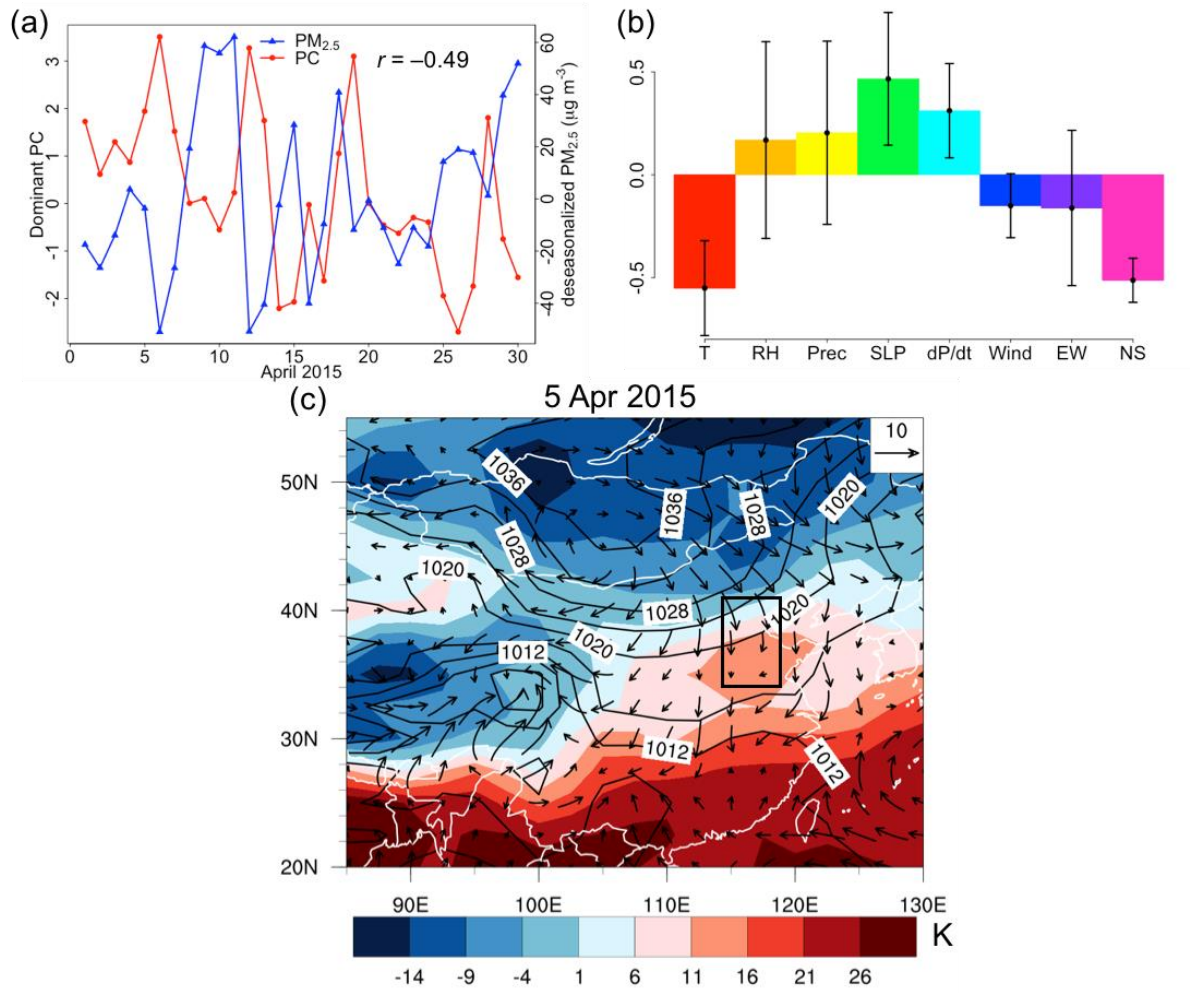

Fig. S5. First springtime dominant meteorological mode for observed $PM_{2.5}$ variability in the Beijing-Tianjin-Hebei (BTH). (a) deseasonalized total $PM_{2.5}$ concentrations and the dominant PC time series in April 2015. (b) composition of this dominant mode as measured by the coefficients α_{kj}, with error bars showing two standard deviations of the distributions. (c-d) synoptic weather maps on 5 Apr 2015, corresponding to the positive influence from the mode, with temperature (K) as shaded colors and SLP (Pa) as contours. The rectangle indicates BTH in the map. The weather map is plotted using NCEP/NCAR reanalysis I data.

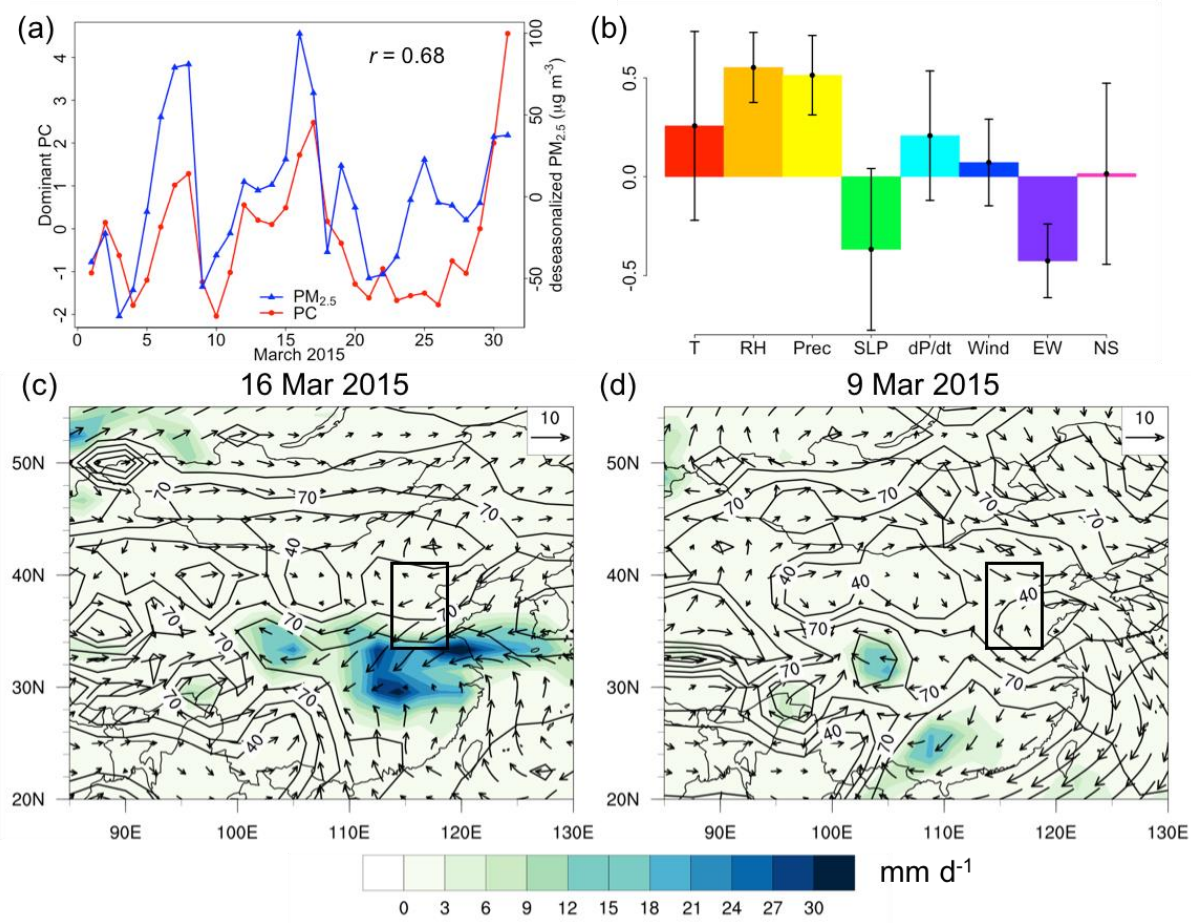

Fig. S6. Second springtime dominant meteorological mode for observed $PM_{2.5}$ variability in the Beijing-Tianjin-Hebei (BTH). (a) deseasonalized total $PM_{2.5}$ concentrations and the dominant PC time series in March 2015. (b) composition of this dominant mode as measured by the coefficients α_{kj}, with error bars showing two standard deviations of the distributions. (c-d) synoptic weather maps on 16 and 9 Mar 2015, corresponding to the positive and negative influences from the mode, with rainfall (mm d^{-1}) as shaded colors, wind speed (m s^{-1}) as vectors and RH (%) as contours. (c) shows the positive influence that characterizes onshore flow with high RH (>70%) but little rainfall over BTH, corresponding to high $PM_{2.5}$ level. (d) shows the negative influence with westerly flow and low RH (~40%). The rectangles indicate BTH in the maps.

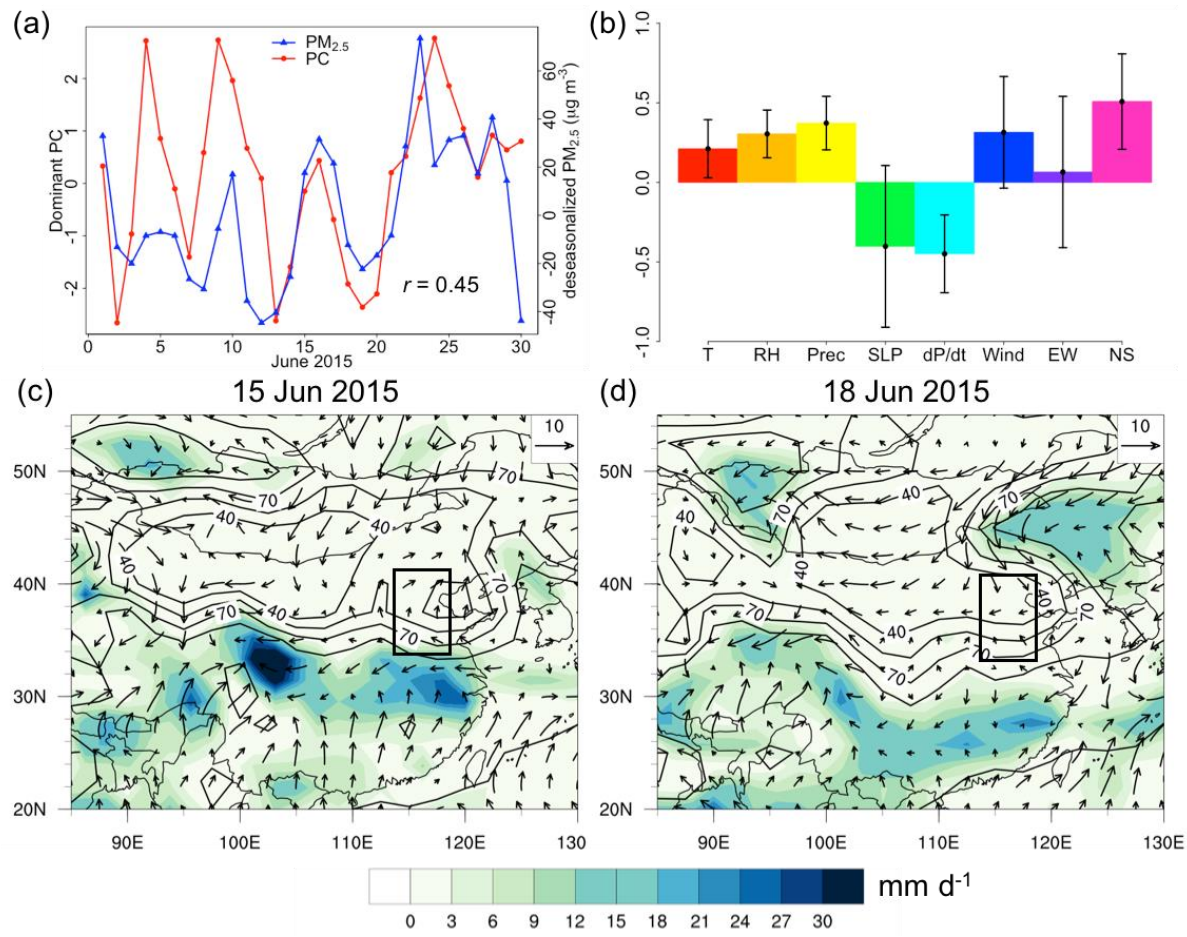

Fig. S7. Summertime dominant meteorological mode for observed $PM_{2.5}$ variability in the Beijing-Tianjin-Hebei (BTH). (a) deseasonalized total $PM_{2.5}$ concentrations and the PC time series in June 2015. (b) composition of this dominant mode as measured by the coefficients α_{kj}, with error bars showing two standard deviations of the distributions. (c-d) synoptic weather maps on 23 and 18 Jun 2015, corresponding to the positive and negative influences from the mode, with rainfall (mm d^{-1}) as shaded colors, wind speed (m s^{-1}) as vectors and RH (%) as contours. (c) shows the positive influence characterized by high RH (>70%), southerly flow and a "Mei-yu" rain belt at the south of BTH. (d) shows the negative influence with northerly flow and low RH (<40%). The rectangles indicate BTH in the maps.

Table S3. Regression results of the principal component time series on $PM_{2.5}$ in the Yangtze River Delta (YRD). Significant results are colored in red. NAs indicate PCs with variance smaller than 1.

Season	$PM_{2.5}$ variability explained (%)				Regression coefficient (μg m^{-3})			
	1st PC	2nd PC	3rd PC	4th PC	1st PC	2nd PC	3rd PC	4th PC
Winter	0.00	4.27	16.99	NA	0.00	–4.95	–11.51	NA
Spring	4.56	4.94	17.09	NA	2.34	–2.36	6.08	NA
Summer	3.01	23.97	10.44	6.64	–2.24	5.17	–4.15	3.27
Fall	0.15	9.41	12.48	NA	–0.18	4.80	6.59	NA
Annual	0.10	5.86	14.46	NA	–0.51	4.16	–7.41	NA

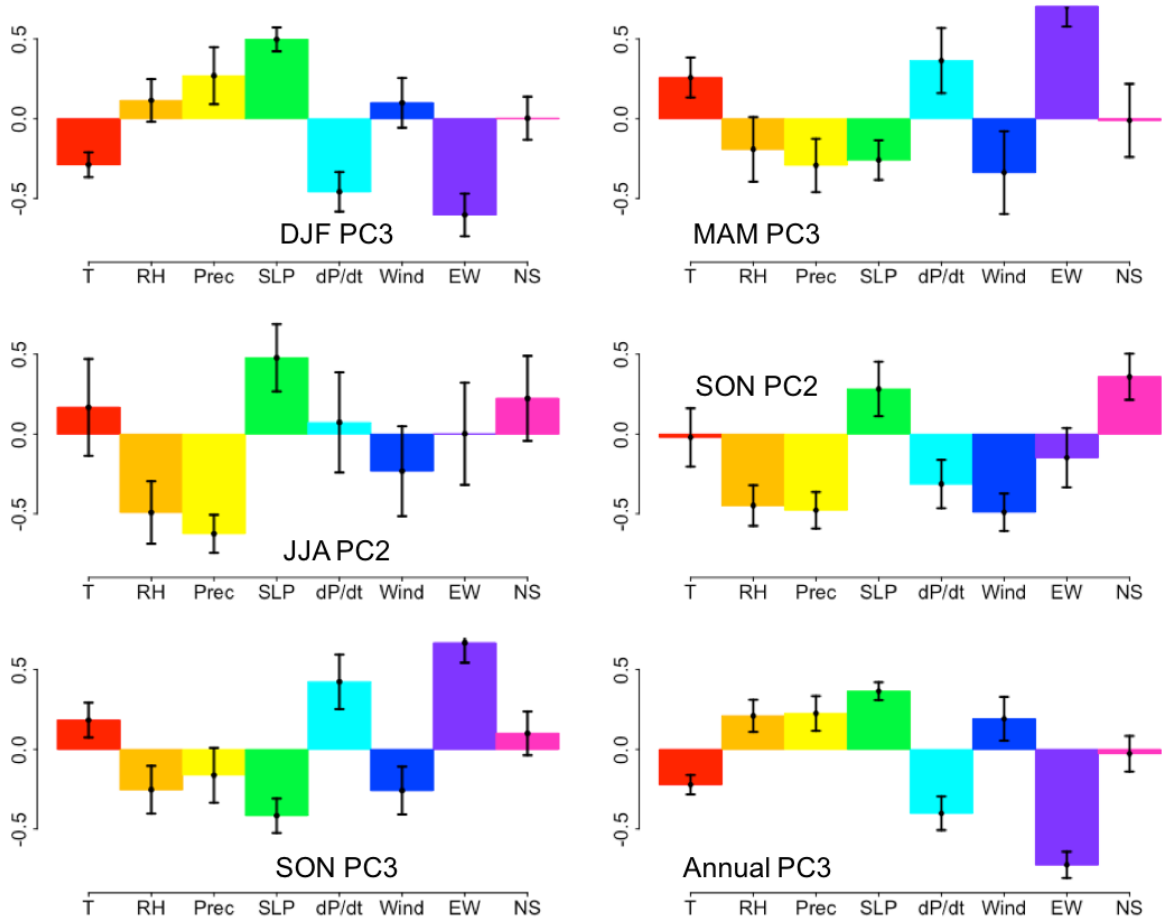

Fig. S8. Empirical orthogonal functions (EOFs) of dominant principal components (PCs) for individual seasons and for whole year in the Yangtze River Delta (YRD), corresponding to the red numbers in Table S3. We classify the second PCs in summer and fall as rain induced by low-pressure troughs or tropical cyclones, and the rest are rainfall associated with onshore flow. Error bars show two standard deviations of the distributions.

3. Seasonally dominant meteorological modes of $PM_{2.5}$ variability in the Yangtze River Delta (YRD)

Apart from onshore flow, YRD is also influenced by fleeting low-pressure systems. Figure S9 shows the summertime dominant mode which explains 24% of the $PM_{2.5}$ variability in summer. The mode has a negative correlation with the deseasonalized $PM_{2.5}$ (Fig. S9a). The EOF (Fig. S9b) indicates that the system contains high RH and intense precipitation, low SLP and northerly wind. Figure S9c shows the weather map on 23 Aug 2015, revealing a deep surface low with minimum SLP of 994 hPa on China sea with highest rainfall of 45 mm d^{-1}. The map suggests that this mode represents a low-pressure trough or tropical storm sweeping from the south in a northeastward direction to YRD. The one on the map is tropical cyclone Goni, which brought 20 mm d^{-1} rainfall as well as northerly wind to YRD. Intense rainfall and strong cyclonic winds washed out $PM_{2.5}$ or advected it away during this event. Figure S8d shows the negative phase of this PC on 25 Aug with mild weather conditions and increasing $PM_{2.5}$. On 11 Aug, there is another positive peak in PC (Fig. S9a), corresponding to tropical cyclone Soudelor, which also depleted $PM_{2.5}$ effectively.

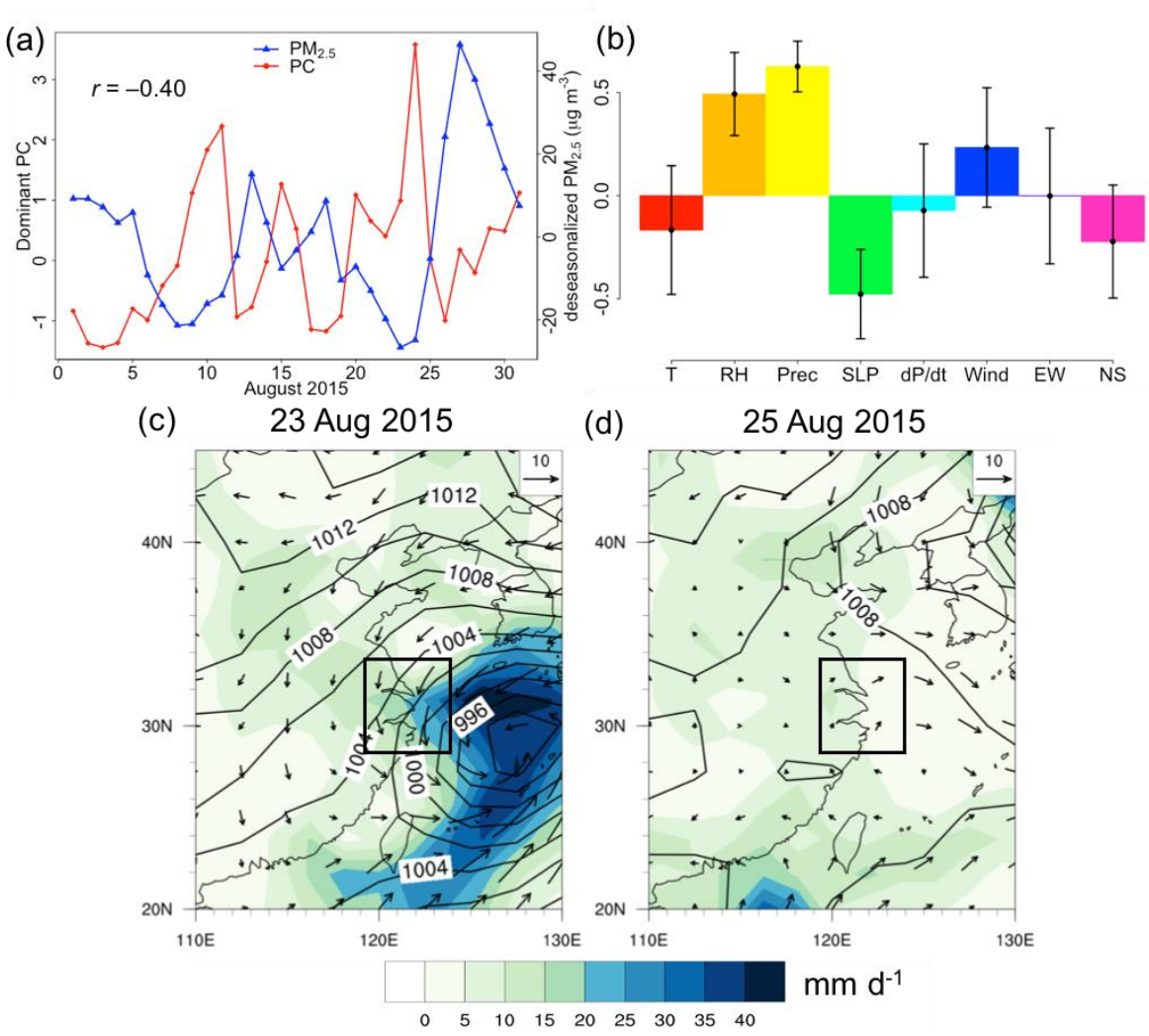

Fig. S9. Dominant meteorological mode for observed $PM_{2.5}$ variability in the Yangtze River Delta (YRD) in summer. (a) deseasonalized total $PM_{2.5}$ concentrations and the PC time series in August 2015. (b) composition of this dominant mode as measured by the coefficients α_{kj}, with error bars showing two standard deviations of the distributions. (c-d) synoptic weather maps on 23 and 25 Aug 2015, corresponding to the positive and negative influences from the mode, with rainfall (mm d^{-1}) as shaded colors, wind speed (m s^{-1}) as vectors and SLP (hPa) as contours. (c) shows the positive influence with a strong low-pressure system or tropical cyclone that corresponds to $PM_{2.5}$ decrease. (d) shows the negative influence corresponding to a mild weather with little rain and wind. The rectangles indicate YRD in the maps.

Table S4. Regression results of the principal component time series on $PM_{2.5}$ in the Pearl River Delta (PRD). Significant results are colored in red. NAs indicate PCs with variance smaller than 1.

Season	$PM_{2.5}$ variability explained (%)			Regression coefficient (μg m^{-3})		
	1st PC	2nd PC	3rd PC	1st PC	2nd PC	3rd PC
Winter	11.22	19.47	2.62	–3.38	–5.84	–2.78
Spring	0.14	21.51	0.75	–0.29	–3.96	–0.95
Summer	17.57	14.73	3.69	–2.67	3.04	1.77
Fall	0.05	24.69	0.96	0.18	–5.57	1.33
Annual	0.57	21.82	2.39	–0.73	4.87	–1.98

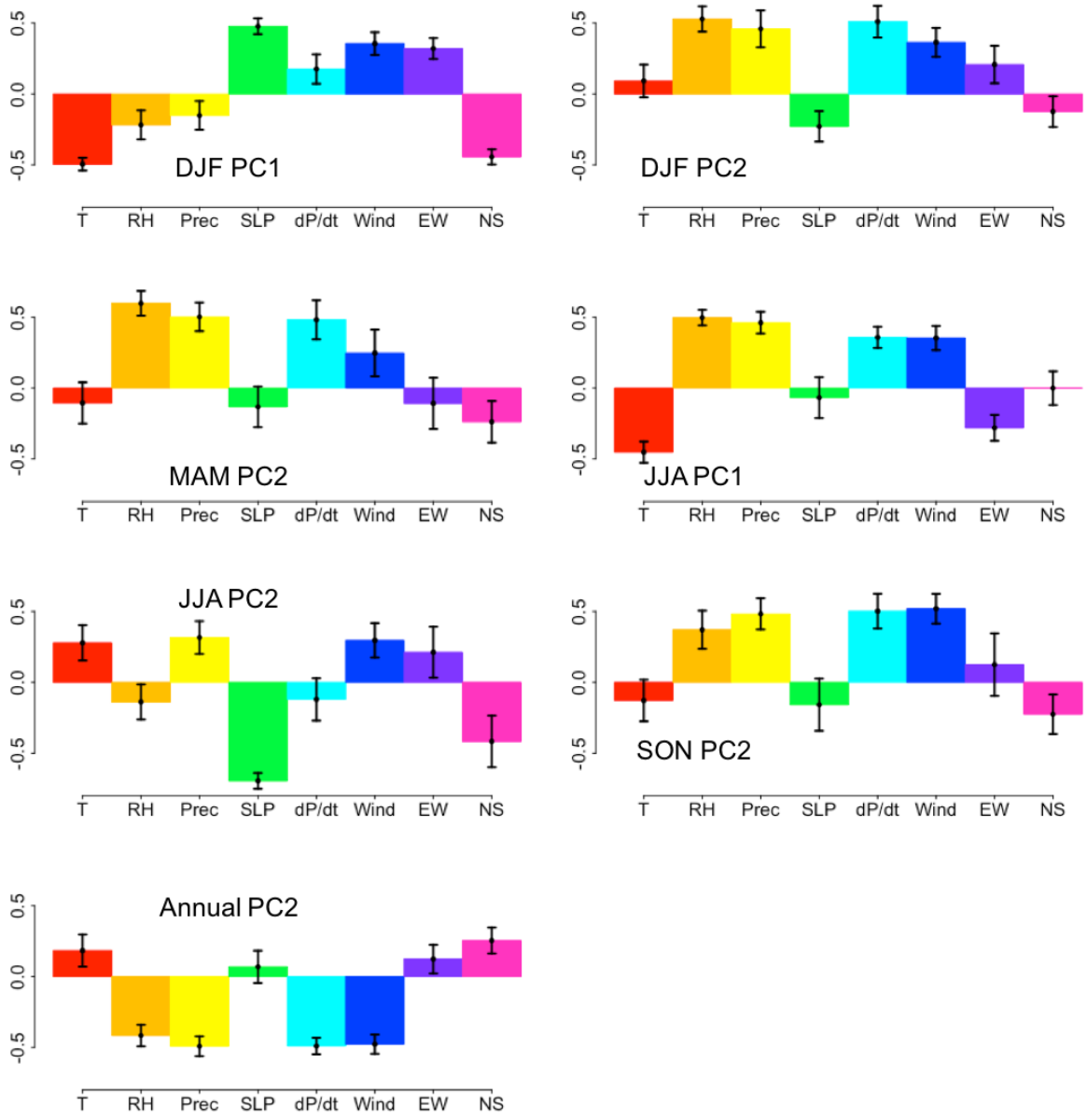

Fig. S10. Empirical orthogonal functions (EOFs) of dominant principal components (PCs) for individual seasons and for whole year in the Pearl River Delta (PRD), corresponding to the red numbers in Table S4. We classify DJF PC1 as cold fronts from Siberian high, JJA PC1 as low-pressure trough with rainfall, JJA PC2 as subsidence inversions created by tropical cyclones, and the other PCs as frontal rain. Error bars show two standard deviations of the distributions.

4. Seasonally dominant meteorological modes of $PM_{2.5}$ variability in the Pearl River Delta (PRD)

There are two modes controlling $PM_{2.5}$ variability in summer, contributing to 11% and 20% of $PM_{2.5}$ variability, respectively. Figure S11 shows the first mode, which has a negative correlation with $PM_{2.5}$ (Fig. S10a) and consists of low temperature, high RH and rainfall, negative SLP anomaly, strong positive pressure tendency and strong easterly wind (Fig. S11b). This mode represents a low-pressure trough located on the South China Sea to the south of PRD, or sometimes a tropical cyclone making landfall to the west of PRD. Figure S11c shows the weather map on 14 Aug 2016, corresponding to the positive phase of the mode. There was a low-pressure system located at the south China sea, accompanying two rainfall extrema to the southeast and southwest of PRD. Strong easterly wind from the ocean associated with cyclonic flow ventilated air pollutants away from PRD during this event. The rainfall system in the east later developed into tropical cyclone Dianmu, which moved westward and made landfall to the west of PRD on 18 Aug 2016. The east quadrant of Dianmu was associated with strong southerly wind (daily mean 15 m s^{-1}) and rain (daily mean 40 mm d^{-1} over PRD), which depleted $PM_{2.5}$ at PRD (Fig. S11a). Figure S10d shows the negative phase of this mode on 23 Aug 2016, characterized by weak wind and some precipitation, with $PM_{2.5}$ slowly accumulating to 40 μg m^{-3} within a week.

Figure S12 shows the second mode for dominating daily $PM_{2.5}$ variability in summer. This mode consists of high temperature, high precipitation, extremely low pressure and northerly wind (Fig. S12b), and has a positive correlation with $PM_{2.5}$. The PC has an overall positive effect on PM, but sometimes also has the opposite impact, as seen in the first few days of July in Fig. S12a. This mode is characterized by a low-pressure system with a strong local minimum of SLP, occasionally representing a brief tropical cyclone or tropical depression. For example, the peaks of the PC on 9 July, 9 and 22 Aug 2016 (Fig. S12a) represent three tropical cyclones (Linfa, Soudelor and Goni), which either made landfalls on the east of PRD or were deflected northeastward. Tropical cyclones approaching the southeastern coast usually induce subsidence inversion over the PRD (Feng et al., 2007; Wang and Kwok, 2003). Sinking motion occurs around the periphery of the cyclone due to strong rising motion of air in the cyclone eye, suppressing planetary boundary layer (PBL) height while causing stagnation and adiabatic heating and drying of atmosphere (e.g., Feng et al., 2007). This mechanism prevents particles from being diluted through PBL mixing or experiencing ventilation, resulting in a pollution episode just before the arrival of the cyclone. As the cyclone moves inland, southwesterly wind

brings rainfall that scavenges the $PM_{2.5}$. Figure S11 also shows weather maps with positive and negative phases of the PC during the influence of tropical cyclone Soudelor. Due to anticlockwise spinning, the Soudelor landfall on 8 Aug 2015 at Fujian brought intense rainfall (110 mm d^{-1}) from Pacific Ocean to the eastern Fujian (Fig. S12c), and the PRD was affected by subsidence at its western periphery. PM accumulated in the region from the end of July to 8 Aug until the arrival of Soudelor. Figure S12d shows that on 26 Jul 2016, a few days before the arrival of Soudelar, SLP was relatively high and westerly wind blew onshore, helping to ventilate PM.

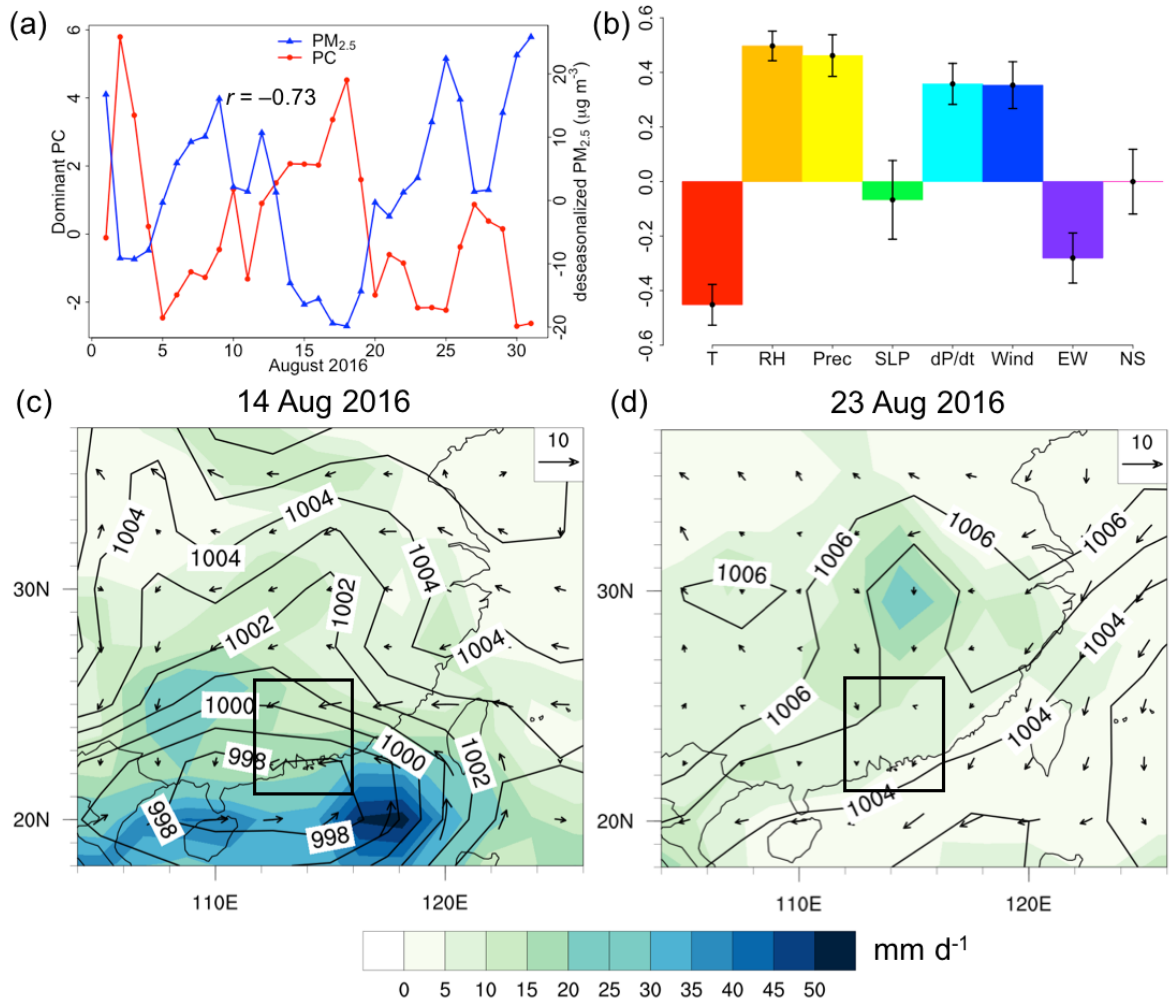

Fig. S11. First summertime dominant meteorological mode for observed $PM_{2.5}$ variability in the Pearl River Delta (PRD). (a) deseasonalized total $PM_{2.5}$ concentrations and the PC time series in August 2016. (b) composition of this dominant mode as measured by the coefficients α_{kj}, with error bars showing two standard deviations of the distributions. (c-d) synoptic weather maps on 14 and 23 Aug 2016, corresponding to the positive and negative influences from the mode, with precipitation (mm d^{-1}) as shaded colors, wind speed (m s^{-1}) as vectors and SLP (hPa) as contours. (c) shows the positive influence with a low-pressure system or tropical cyclone sweeping across PRD, bringing substantial rainfall and strong wind that depletes $PM_{2.5}$. (d) shows the negative influence with a mild weather over PRD. The rectangles indicate PRD in the maps.

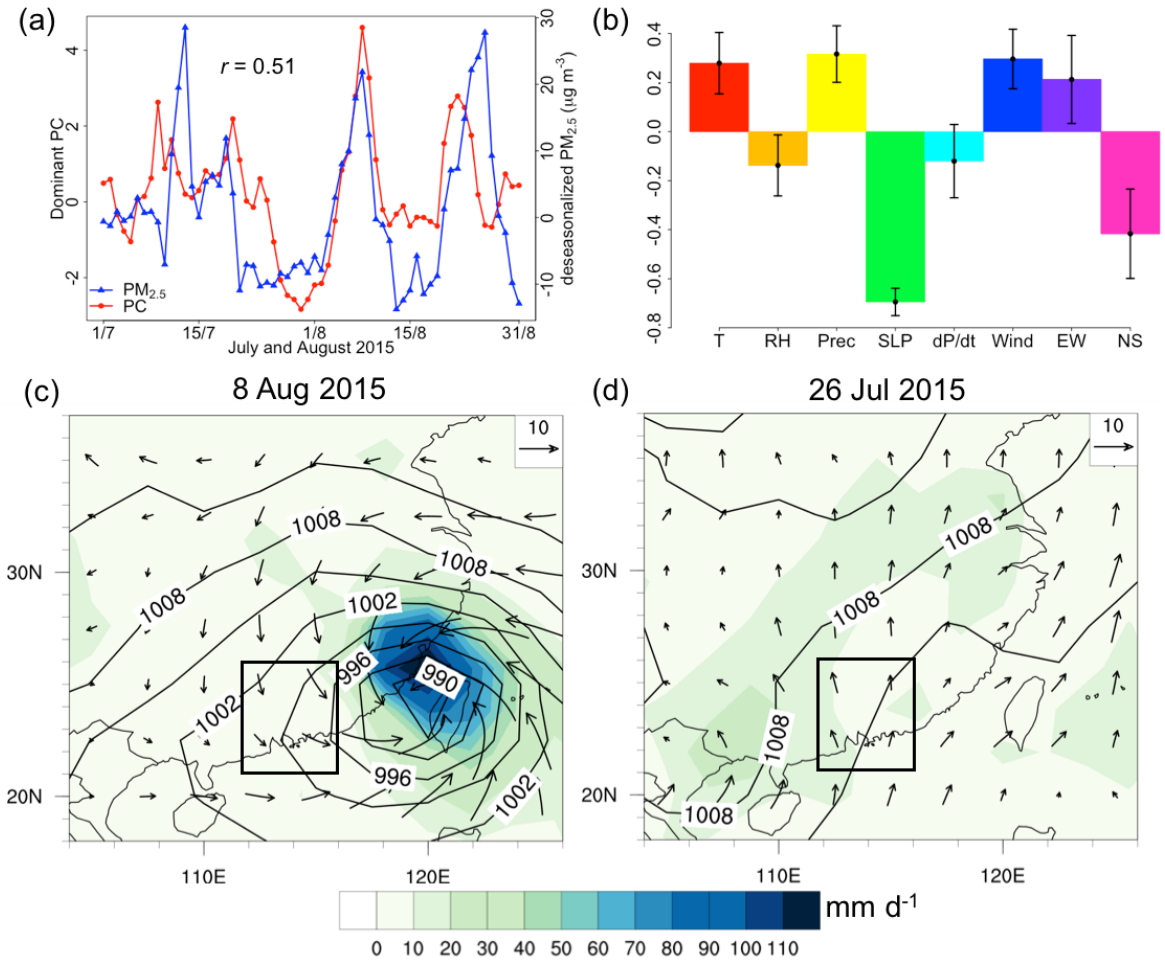

Fig. S12. Second summertime dominant meteorological mode for observed $PM_{2.5}$ variability in the Pearl River Delta (PRD). (a) deseasonalized total $PM_{2.5}$ concentrations and the PC time series in July and August 2015. (b) composition of this dominant mode as measured by the coefficients α_{kj}, with error bars showing two standard deviations of the distributions. (c-d) synoptic weather maps on 8 Aug and 26 Jul 2015, corresponding to the positive and negative influences from the mode, with precipitation (mm d^{-1}) as shaded colors, wind speed (m s^{-1}) as vectors and sea level pressure (hPa) as contours. (c) shows the positive influence with a low or tropical cyclone making landfall to the east of PRD, such that PRD is under the subsidence inversion created by the cyclone. (d) shows the negative influence with southerly flow to PRD that ventilates pollution. The rectangles indicate PRD in the maps.

Table S5. Regression results of the principal component time series on $PM_{2.5}$ in the Sichuan Basin (SCB). Statistically significant results are colored in red. NAs indicate PCs with variance smaller than 1.

Season	$PM_{2.5}$ variability explained (%)			Regression coefficient (μg m^{-3})		
	1st PC	2nd PC	3rd PC	1st PC	2nd PC	3rd PC
Winter	17.69	22.15	3.96	–9.13	11.51	–6.64
Spring	15.94	25.62	0.86	–4.61	5.78	–1.60
Summer	3.12	26.93	5.75	1.34	3.73	–2.37
Fall	0.21	28.12	NA	–0.55	–7.07	NA
Annual	8.78	24.61	2.77	–4.52	7.57	–3.62

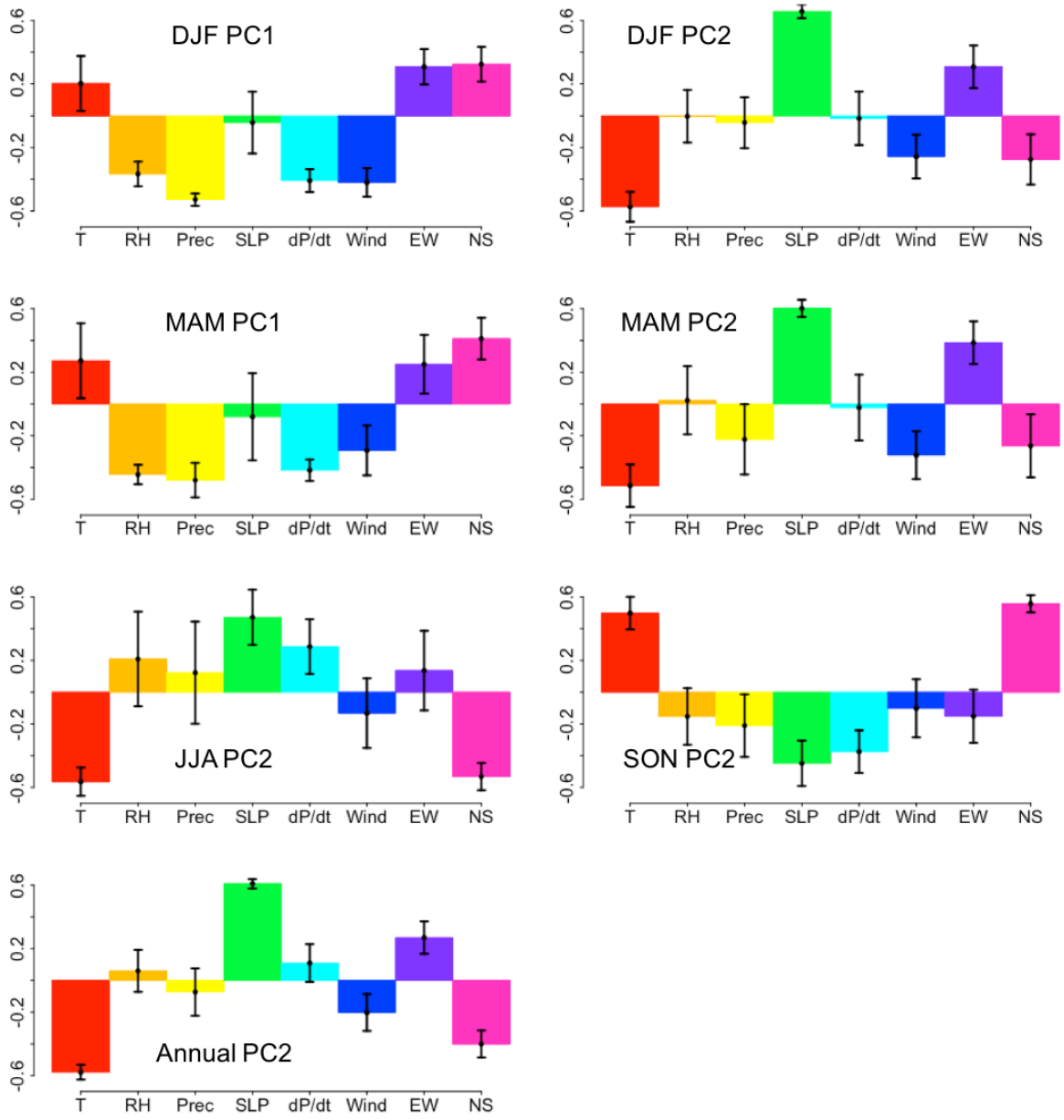

Fig. **S13**. Empirical orthogonal functions (EOFs) of dominant principal components (PCs) for individual seasons and for whole year in the Sichuan Basin (SCB), corresponding to the red numbers in Table S5. We classify the EOFs of the first PCs in DJF and MAM as frontal rain, and the rests are classified as northerly flow from Siberian high. Error bars show two standard deviations of the distributions.

5. Seasonally dominant meteorological modes of $PM_{2.5}$ variability in the Sichuan Basin (SCB)

Besides the northerly flow originating from the Siberian high, a second mode drives $PM_{2.5}$ variability in DJF and MAM (Table S5). Figure S14 shows this mode in spring, which has an overall correlation with $PM_{2.5}$ of $r = -0.42$ (Fig. S14a). This mode is associated with low temperature, high RH and rainfall, strong pressure tendency and strong northeasterly wind (Fig. S14b), which resembles the EOF in Fig. 5b. This mode also represents a cold-frontal rain system. Figure S14c shows a weather map of this mode's positive phase on 18 Apr 2015. A cold front from the north to SCB caused as much as 35 mm d^{-1} over central China, which led to $PM_{2.5}$ decreasing by 60 μg m^{-3} over the SCB within two days. During the negative phase of this mode on 14 Apr 2015 (Fig. S14d), there was little rain and wind in SCB, which favored the gradual accumulation of $PM_{2.5}$.

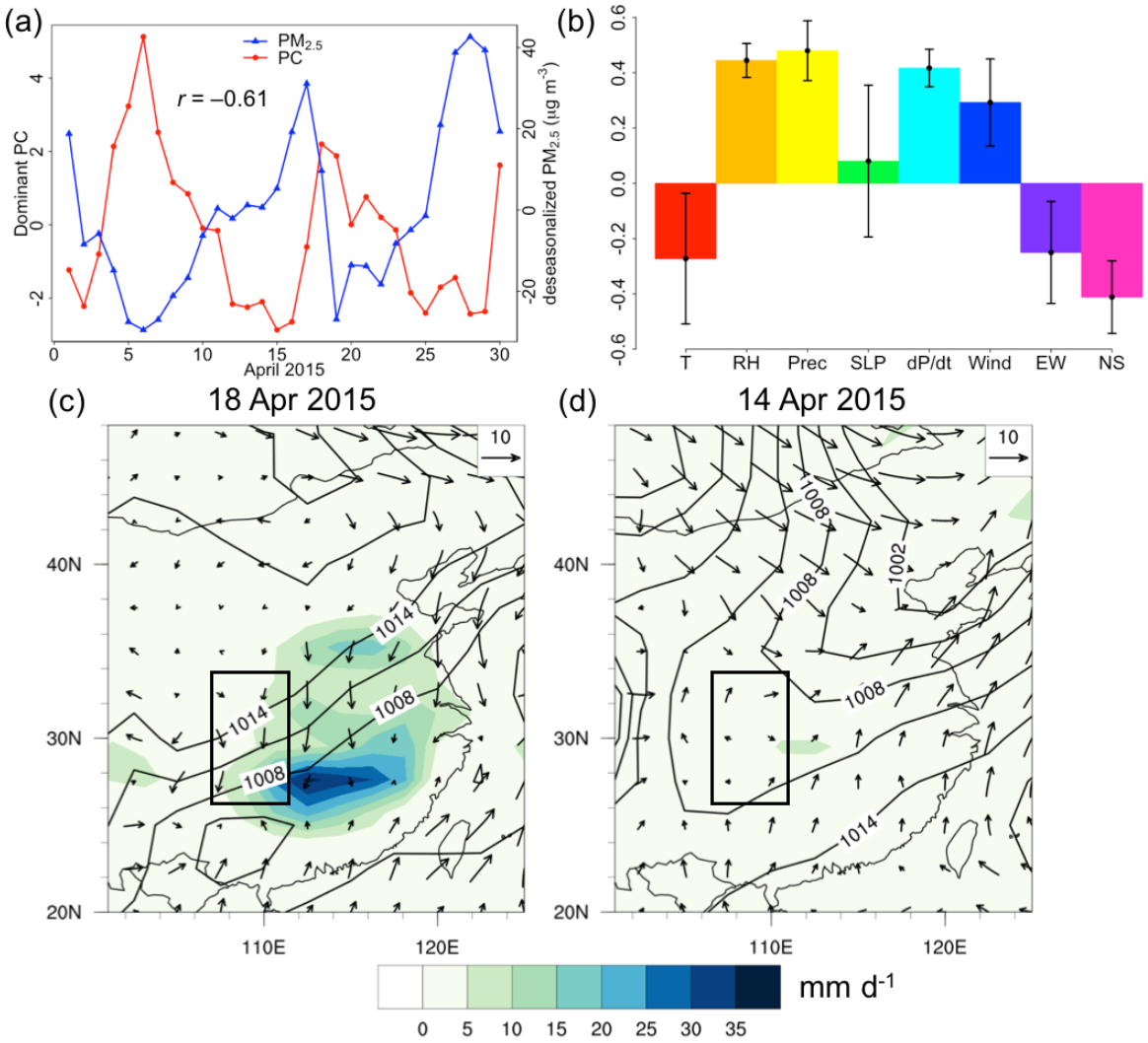

Fig. S14. First springtime dominant meteorological mode for observed $PM_{2.5}$ variability in the Sichuan Basin (SCB). (a) deseasonalized total $PM_{2.5}$ concentrations and the PC time series in April 2015. (b) composition of this dominant mode as measured by the coefficients α_{kj}, with error bars showing two standard deviations of the distributions. (c-d) synoptic weather map on 18 and 14 Apr 2015, corresponding to the positive and negative influences from the mode, with precipitation (mm d^{-1}) as shaded colors, wind speed (m s^{-1}) as vectors and sea level pressure (hPa) as contours. (c) shows the positive influence that characterizes northerly flow with rainfall, while (d) shows negative influence with mild weather. The rectangles indicate SCB in the maps.

References

Dawson, J. P., Adams, P. J., and Pandis, S. N.: Sensitivity of $PM_{2.5}$ to climate in the Eastern US: a modeling case study. *Atmos. Chem. Phys.*, *7*(16), 4295–4309, 2007b.

Feng, Y., Wang, A., Wu, D., and Xu, X.: The influence of tropical cyclone Melor on PM_{10} concentrations during an aerosol episode over the Pearl River Delta region of China: numerical modeling versus observational analysis. *Atmos. Environ.*, *41*(21), 4349–4365, 2007.

van Donkelaar, A., Martin, R. V., Brauer, M., Hsu, N. C., Kahn, R. A., Levy, R. C., Lyapustin, A., Sayer, A. M. and Winker, D. M.: Global estimates of fine particulate matter using a combined geophysical-statistical method with information from satellites, models, and monitors. *Environ. Sci. Technol.*, *50*(7), 3762–3772, 2016.

Wang, T., and Kwok, J. Y.: Measurement and analysis of a multiday photochemical smog episode in the Pearl River Delta of China. *J. Appl. Meteorol.*, *42*(3), 404-416, 2003.

Zhao, P., Zhang, R., Liu, J., Zhou, X. and He, J.: Onset of southwesterly wind over eastern China and associated atmospheric circulation and rainfall. *Climate Dyn.*, 28(7–8), 797–811, 2007.